Interfacial tension controlled fusion of individual femtolitre droplets and triggering of confined chemical reactions on demand†

Seung-Yong Jung,[a] Scott T. Retterer[ab] and C. Patrick Collier*[a]

Received 4th September 2010, Accepted 11th October 2010
DOI: 10.1039/c0lc00376j

This paper describes stepwise on-demand generation and fusion of femtolitre aqueous droplets based on interfacial tension. Sub-millisecond reaction times from droplet fusion were demonstrated, as well as a reversible chemical toggle switch based on alternating fusion of droplets containing acidic or basic solution, monitored with the pH-dependent emission of fluorescein.

Controlled fusion of two or more water-in-oil microdroplets with droplet-based microfluidics has enabled precise control in initiating chemical and biochemical reactions in compartmentalized biomimetic reactors in areas including single-molecule enzymatic assays, protein crystallization, gene expression and nanoparticle synthesis.[1–5] Both passive and active approaches for controlling droplet fusion have been reported. "Active" methods rely on mechanical, optical or electrical assistance in co-locating droplets and fusing them together.[6–21] "Passive" methods rely on microfabricated device structure, and hydrodynamic variables such as flow rates and flow instabilities induced by interfacial tension or viscosity to induce fusion.[22–37]

Most droplet-based microfluidic platforms, for example, microfluidic chips employing flow focusing and T-junction geometries, generate aqueous droplets or plugs in continuous water-in-oil segmented flows.[13–37] Droplets are generated at high flow rates, necessitating precise temporal and spatial synchronization in order to coalesce two or more droplets in a controlled and reproducible manner. On the other hand, on-demand strategies for droplet generation and coalescence target a specific pair of selected droplets for fusion, subsequent manipulation and interrogation.[6–12] Both active and passive control mechanisms for fusion of droplets generated in continuous segmented flows have been reported. However, on-demand droplet generation methods have employed only active mechanisms to control fusion to date.

We recently described a passive method for on-demand droplet formation based only on interfacial tension-induced forces resulting from an abrupt change in channel height at a microfabricated water–oil junction.[38] Monodisperse, femtolitre volume aqueous droplets could be generated one at a time on demand with the application of timed pressure pulses. The magnitude of shear stresses involved in droplet splitting at the junction orifice was significantly less than the relatively high shearing instabilities used to split off ultrasmall (sub-pL) droplets in continuous segmented flows.[39]

Here, we build on that result by including a second droplet generating channel to facilitate on-demand production and fusion of multiple femtolitre aqueous droplets. Using this system, fusion and reaction initiation times on the order of one millisecond or less are demonstrated, as determined by the precipitation of insoluble AgCl(s) from the bimolecular reaction of $AgNO_3$(aq) and NaCl(aq). Dilution of a droplet containing fluorescent beads from fusion with a droplet containing buffer showed that mixing times had both convective and diffusive components. Finally, we demonstrate the utility of passive on-demand droplet fusion by creating a reversible chemical toggle switch based on the pH-dependent fluorescence of fluorescein. Alternating "digital" aliquots of monodisperse femtolitre droplets containing either acidic or basic solution were used to turn fluorescence of the switch "on" and "off". This methodology is simpler than active control methods for manipulating and fusing droplets on demand.

Fig. 1A is a schematic of the device. Two apposed (1 μm wide × 1 μm high) microchannels fabricated in poly(dimethylsiloxane) (PDMS) were designed to deliver separate droplets containing different aqueous reagents into a larger center oil channel (18 μm high, with widths varying from about 7 μm to 14 μm). Fabrication details were described previously[38] and are supplemented in the ESI†. Fig. 1B is a scanning electron microscopy (SEM) image showing the

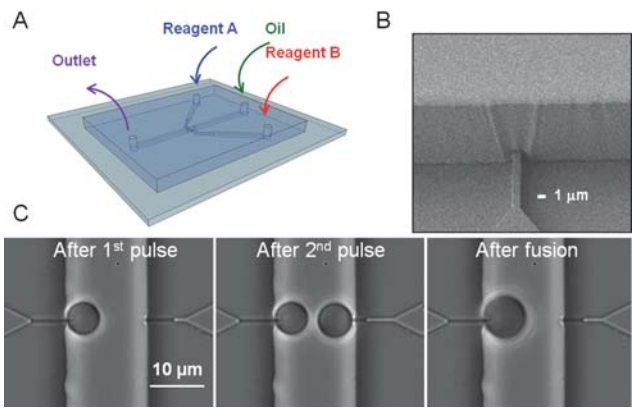

Fig. 1 (A) Schematic of the microfluidic device used to generate and fuse together two femtolitre water-in-oil droplets on demand, consisting of two apposed 1 μm × 1 μm aqueous microchannels intersecting a larger oil channel. (B) SEM inset showing detail of the height difference between an aqueous and oil channel on the silicon master used to form the PDMS replica (adapted from ref. 38). (C) Still images captured with CCD camera of consecutive formation of droplets and fusion.

[a]*Center for Nanophase Materials Sciences, Oak Ridge National Laboratory, Oak Ridge, Tennessee, 37831, USA. E-mail: colliercp@ornl.gov*
[b]*Biological and Nanoscale Systems Group, Biosciences Division, Oak Ridge National Laboratory, Oak Ridge, TN, 37831-6445, USA*

† Electronic supplementary information (ESI) available: Device fabrication and experimental details, droplet shrinkage rates, droplet size distributions as functions of oil channel width, CCD images of formation of silver granules, two dimensional fluorescence distributions corresponding to Fig. 3, bright field movie sequences of acidic and basic droplet fusion events for Fig. 4. See DOI: 10.1039/c0lc00376j

detail of the junction between the aqueous and oil channels on the silicon master used to form the PDMS replica, highlighting the difference in channel height at the water–oil junction.

To prevent wetting of the aqueous droplets on the channel walls, PDMS replicas were bonded to PDMS-coated glass cover slips, followed by heating at 120 °C for 48 hours to ensure complete hydrophobic recovery. Shrinkage of aqueous droplets from evaporation was minimized by purifying the soybean oil used as the immiscible carrier phase to reduce surface-active contaminants, which reduces the partitioning of water into the oil.[40] Evaporation was further reduced by saturating the PDMS chip in deionized water for at least 24 hours prior to experiments. Droplet shrinkage rates were 1 μm^2 min^{-1} over the time course of a typical experiment (about an hour).

On-demand generation of droplets was triggered by short (10 ms) pressure pulses with magnitudes about 5% higher than the capillary pressure necessary to fill a (1 μm × 1 μm) hydrophobic PDMS microchannel with aqueous solution up to the junction with the oil channel (124–131 kPa). While an abrupt change in channel height at the aqueous/oil channel junction was required to generate droplets on demand, the width of the oil channel was not as important a factor for droplet formation. From bright field images of 87 droplets taken with a CoolSNAP HQ CCD camera (Roper Scientific), the droplet size distribution for devices with the 7.3 μm wide oil channels was 3.7 ± 0.4 μm (from 37 images), and 5.5 ± 0.6 μm for devices with 14.6 μm wide oil channels (from 50 images). These distributions may be found in the ESI†. Careful balancing of the hydrostatic pressure in the oil channel enabled precise positioning of the first droplet to within 1.1 ± 0.6 μm (from 45 images) of the orifice without crossflow of the oil phase, as shown in the first panel of Fig. 1C.

Simultaneous generation and fusion of droplets from the two aqueous channel openings with synchronized pressure pulses were difficult due to coupled pressure-induced flow fluctuations between the channels. Instead, droplets could be ejected from either aqueous channel, and forced to collide and fuse with a droplet already located in the oil channel. This process is shown in the second and third panels of Fig. 1C. The magnitudes of the 10 ms pressure pulses used to eject subsequent droplets were slightly higher than those used to form the first droplet (by about 2 kPa) in order to impart additional kinetic energy to facilitate fusion and mixing. At the completion of each fusion event, the channel junction could be cleared of droplets for the next experiment by temporarily increasing the pressure in the oil channel to about 40 kPa.

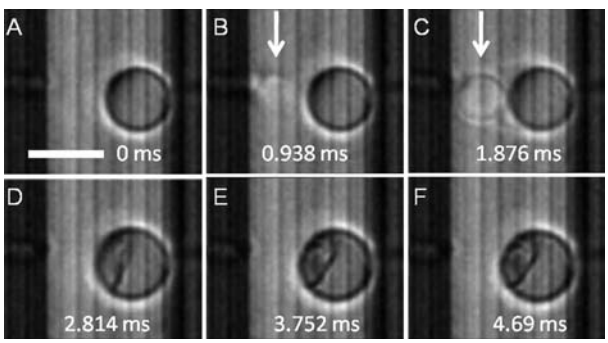

Fig. 2 (A–F) Still images captured with high-speed CMOS camera of fusion of initial 2 M NaCl(aq) droplet with subsequent 2 M $AgNO_3$(aq) droplet (arrows). Frame rate 938 μs. Scale bar 5 μm.

Fig. 2A–F is a sequence of bright field images from a high-speed CMOS camera (EPIX SV643) showing the formation of AgCl(s) after fusion of a droplet containing 2 M NaCl(aq) with one containing 2 M $AgNO_3$(aq).[6] The NaCl(aq) droplet detached first from the right hand side channel, as seen in Fig. 2A. In Fig. 2B and C, the second $AgNO_3$(aq) droplet can be observed forming in the oil channel from the left, and colliding with the NaCl(aq) droplet before it could fully inflate and detach from its channel opening. Within the time period of one frame, Fig. 2C and D, corresponding to less than 1 ms, the $AgNO_3$(aq) droplet completely merged with the larger NaCl(aq) droplet, and the formation of a gel-like film containing AgCl(s) appeared to be largely complete. No transient shape changes beyond an increase in droplet diameter were observed after fusion, indicating that the timescale for these effects must be shorter than 1 ms. The last two images in the sequence show little additional changes to the gel.[41] The fact that the AgCl(s) product was located on only one side of the fused droplet indicates the precipitation rate was faster than any mixing time scales in the droplet. Product formation was considerably faster than the estimated diffusive mixing time, which would be on the order of 10 ms, using $t_{mix} = \langle x^2 \rangle / 2D$ in a 5 μm diameter product droplet as an estimate, and using the published diffusion coefficient for 2 M $AgNO_3$(aq) of about 10^3 μm^2 s^{-1}.[42]

To obtain a clearer picture of the relative roles of convective *versus* diffusive mixing triggered by droplet fusion, we measured the time-dependent change in fluorescence intensity from a droplet containing 50 nm diameter fluorescent polymer microspheres (FS02F/9290, Bangs Laboratories) in phosphate buffer as it merged with a droplet containing only buffer solution, shown in Fig. 3. The much slower diffusion coefficient of the microspheres, 8.4 μm^2 s^{-1},[43] allowed us to track changes in fluorescence intensity after droplet fusion at the 100 ms frame rate of the CCD camera, comparable to diffusive mixing time scales of the beads. Droplet sizes before (left inset, 5.4 ± 0.3 μm) and after fusion (right inset, 6.5 ± 0.2 μm) were estimated from full width at half maxima of fluorescent intensity line profiles of images taken from movie sequences of droplet fusion captured with the CCD camera. Two dimensional analyses of the fluorescence distribution of the droplet containing microspheres did not show any transient shape changes after fusion (see ESI†).

The time-dependent change in fluorescence due to dilution of the microspheres was determined by measuring the average intensity

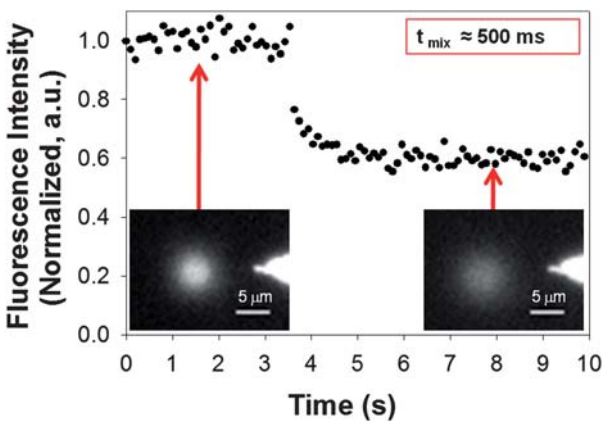

Fig. 3 Fluorescence intensity decrease of droplet containing 50 nm microspheres (0.4 mg mL^{-1} in phosphate buffer, pH 7.2) before (left inset) and after fusion (right inset) with droplet containing only buffer solution.

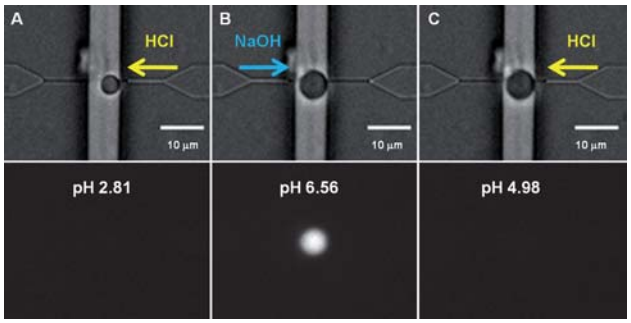

Fig. 4 Operation of reversible chemical toggle switch based on consecutive fusion of droplets containing acidic or basic solution, measured with fluorescence. Top row bright field images and bottom row corresponding fluorescence images. (A) Initial droplet with fluorescein/HCl(aq) at pH 2.81 (right arrow). (B) After fusion with 2 mM NaOH(aq) droplets (left arrow), pH now 6.56. (C) After fusion with HCl(aq) droplet (right arrow), final pH 4.98.

from a 1.7 μm × 1.7 μm region located at the center of each of the fluorescent droplets. The time interval observed between the sharp drop from the initial fluorescent intensity from the unfused droplet and one standard deviation from the mean value of the final intensity after dilution of the microspheres was 500 ms. This is about a factor of 5 faster than the $t_{mix} = \langle x^2 \rangle / 2D = 2.4$ s estimated for diffusive mixing in the product droplet. As a check, the average value of the relative fluorescence intensity after droplet fusion, 61%, was close to the change in concentration of the beads estimated from the change in droplet volume before (82 fL) and after fusion (147 fL), 56%.

In Fig. 4, we show how consecutive fusion operations with droplets containing acidic or basic solutions can rapidly and reversibly switch "on" and "off" the fluorescent intensity of a pH-sensitive dye. Fluorescein in aqueous solution can exist in several ionization forms, cationic, neutral, monoanionic and dianionic, resulting in absorption and fluorescence properties that depend sensitively on pH.[44] The dianion has the strongest fluorescence intensity with a quantum yield of 0.93, while the other forms are significantly less fluorescent.[45] The top row in Fig. 4 shows still images from bright field movie sequences captured with the CCD camera of droplet generation and fusion alternating between an aqueous channel containing 10 μM fluorescein in 2 mM HCl(aq) at pH 2.81 (right hand side channel) and 2 mM NaOH(aq) at pH 11.23 (left hand side channel). The movie sequences are included in the ESI†. The bottom row is fluorescent images displayed with the same maximum and minimum contrast values captured immediately after each corresponding bright field image in the top row.

The chemical toggle switch was initialized in Fig. 4A with the generation and localization in the oil channel of a 42 fL droplet from the fluorescein/HCl(aq) channel at pH 2.81. At this pH, an equilibrium exists between the cationic and neutral forms of fluorescein, related by the polyprotic acid dissociation constant $pK_1 = 2.08$. In Fig. 4B, two 50 fL droplets of the NaOH(aq) solution from the left hand side channel fused with the acidic droplet in the oil channel, increasing its volume to 142 fL. The corresponding fluorescence image shows strong emission emanating from the fusion product. The pH in the fused droplet was estimated by mixing the fluorescein/HCl(aq) and NaOH(aq) solutions at the same volumetric ratios in the bulk as calculated from the size of the droplets, and measuring the pH with a pH meter (S20 SevenEasy, Mettler Toledo), which gave a value of 6.56. At this pH, the major equilibrium species present in the droplet were now the monoanionic and strongly fluorescent dianionic forms ($pK_3 = 6.43$). Addition of another 30 fL droplet from the acidic channel in Fig. 4C decreased the pH of the switch to 4.98 (total volume of the fusion product droplet now 172 fL), corresponding to the neutral form and the monoanion ($pK_2 = 4.31$), neither of which as strongly fluorescent as the dianion. The switch could be reset simply by flushing the aqueous droplet out of the oil channel and reinitializing the sequence of droplet formation and fusion events.

This paper describes a passive method for on-demand control of femtolitre-volume droplet formation and fusion, based on interfacial-induced forces that act on droplets due to an abrupt change in channel height at water/oil channel junctions. We show that chemical reactions due to droplet fusion could be triggered at sub-ms time scales. Although we could not directly image droplet distortion during fusion due to the finite temporal resolution of the cameras used, we determined that mixing triggered by a fusion event is more rapid than can be explained assuming only diffusive contributions, and must also include convection from inertial effects occurring during droplet collisions. Inclusion of surfactants or surface active solutes will stabilize droplets against fusion and slow down droplet fusion dynamics,[36] to the point where real time imaging of transient droplet shape changes may become possible. In addition to control of droplet fusion, this method may enable precise control of droplet separation without fusing in order to quantitatively study the diffusion of molecules across the oil/water interfaces separating the droplets.[46] The demonstration here of a reversible chemical toggle switch based on alternating fusion of droplets containing acidic or basic solution, monitored with the pH-dependent emission of fluorescein, lays the groundwork for exploring more complex chemical and biochemical reaction sequences triggered and monitored in real time in discrete ultrasmall reactors.

Acknowledgements

Support for device fabrication provided by the Center for Nanophase Materials Sciences, which is sponsored by the Scientific User Facilities Division, Office of Basic Energy Sciences, US Department of Energy. Device characterization and analysis were sponsored by the Laboratory Directed Research and Development Program of Oak Ridge National Laboratory, managed by UT-Battelle, LLC, for the US Department of Energy under Contract No. DE-AC05-00OR22725.

Notes and references

1 S.-Y. Teh, R. Lin, L.-H. Hung and A. P. Lee, *Lab Chip*, 2008, **8**, 198–220.
2 (*a*) H. Song, D. L. Chen and R. F. Ismagilov, *Angew. Chem., Int. Ed.*, 2006, **45**, 7336–7356; (*b*) D. T. Chiu and R. M. Lorenz, *Acc. Chem. Res.*, 2009, **42**, 649–658.
3 D. T. Chiu, R. M. Lorenz and G. D. M. Jeffries, *Anal. Chem.*, 2009, **81**, 5111–5118.
4 Y. Schaerli and F. Hollfelder, *Mol. BioSyst.*, 2009, **5**, 1392–1404.
5 H. H. Gorris and D. R. Walt, *Angew. Chem., Int. Ed.*, 2010, **49**, 3880–3895.
6 R. M. Lorenz, J. S. Edgar, G. D. M. Jeffries and D. T. Chiu, *Anal. Chem.*, 2006, **78**, 6433–6439.
7 J. Xu and D. J. Attinger, *J. Micromech. Microeng.*, 2008, **18**, 065020.

8 M. A. Holden, D. Needham and H. Bayley, *J. Am. Chem. Soc.*, 2007, **129**, 8650–8655.
9 W. L. Hwang, M. Chen, B. Cronin, M. A. Holden and H. Bayley, *J. Am. Chem. Soc.*, 2008, **130**, 5870–5879.
10 J. Tang, A. M. Jofre, G. M. Lowman, R. B. Kishore, J. E. Reiner, K. Helmerson, L. S. Goldner and M. E. Greene, *Langmuir*, 2008, **24**, 4975–4978.
11 J. Tang, A. M. Jofre, R. B. Kishore, J. E. Reiner, M. E. Greene, G. M. Lowman, J. S. Denker, C. C. C. Willis, K. Herlmerson and L. S. Goldner, *Anal. Chem.*, 2009, **81**, 8041–8047.
12 L. S. Goldner, A. M. Jofre and J. Tang, in *Methods in Enzymology*, ed. N. G. Walter, Elsevier, Amsterdam, 1st edn, 2010, vol. 472, ch. 5, pp. 61–88.
13 K. Ahn, J. Agresti, H. Chong, M. Marquez and D. A. Weitz, *Appl. Phys. Lett.*, 2006, **88**, 264105.
14 M. Zagnoni and J. M. Cooper, *Lab Chip*, 2009, **9**, 2652–2658.
15 S. Zeng, B. Li, X. Su, J. Qin and B. Lin, *Lab Chip*, 2009, **9**, 1340–1343.
16 W. Wang, C. Yang and C. M. Li, *Small*, 2009, **5**, 1149–1152.
17 L. M. Fidalgo, G. Whyte, D. Bratton, C. F. Kaminski, C. Abell and W. T. S. Huck, *Angew. Chem., Int. Ed.*, 2008, **47**, 2042–2045.
18 W. Wang, C. Yang and C. M. Li, *Lab Chip*, 2009, **9**, 1504–1506.
19 D. R. Link, E. Grasland-Mongrain, A. Duri, F. Sarrazin, Z. Cheng, G. Cristobal, M. Marquez and D. A. Weitz, *Angew. Chem., Int. Ed.*, 2006, **45**, 2556–2560.
20 L. Mazutis, J.-C. Baret, P. Treacy, Y. Skhiri, A. F. Araghi, M. Ryckelynck, V. Taly and A. D. Griffiths, *Lab Chip*, 2009, **9**, 2902–2908.
21 W. Wang, C. Yang, Y.-S. Liu and C. M. Li, *Lab Chip*, 2010, **10**, 559–562.
22 A. M. Skelley, O. Kirak, H. Suh, R. Jaenisch and J. Voldman, *Nat. Methods*, 2009, **6**, 147–152.
23 J. Sivasamy, Y. C. Chim, T.-N. Wong, N.-T. Nguyen and L. Yobas, *Microfluid. Nanofluid.*, 2010, **8**, 409–416.
24 J. Hong, M. Choi, A. J. deMello and J. B. Edel, *BioChip J.*, 2009, **3**, 203–207.
25 J. Hong, M. Choi, J. B. Edel and A. J. deMello, *Lab Chip*, 2010, **10**, 2702–2709.
26 L.-H. Hung, K. M. Choi, W.-Y. Tseng, Y.-C. Tan, K. J. Shea and A. P. Lee, *Lab Chip*, 2006, **6**, 174–178.
27 Y.-C. Tan, J. S. Fisher, A. I. Lee, V. Cristini and A. P. Lee, *Lab Chip*, 2004, **4**, 292–298.
28 T. Teshima, H. Ishihara, K. Iwai, A. Adachi and S. Takeuchi, *Lab Chip*, 2010, **10**, 2443–2448.
29 Y. Bai, X. He, D. Liu, S. N. Patil, D. Bratton, A. Huebner, F. Hollfelder, C. Abell and W. T. S. Huck, *Lab Chip*, 2010, **10**, 1281–1285.
30 L. M. Fidalgo, C. Abell and W. T. S. Huck, *Lab Chip*, 2007, **7**, 984–986.
31 L. Mazutis, J.-C. Baret and A. D. Griffiths, *Lab Chip*, 2009, **9**, 2665–2672.
32 X. Niu, S. Gulati, J. B. Edel and A. J. deMello, *Lab Chip*, 2008, **8**, 1837–1841.
33 C. Priest, S. Herminghaus and R. Seeman, *Appl. Phys. Lett.*, 2006, **88**, 024106.
34 B.-J. Jin, Y. W. Kim and J. Y. Yoo, *J. Micromech. Microeng.*, 2010, **20**, 035003.
35 D. Chen, W. Du, Y. Liu, W. Liu, A. Kuznetsov, F. E. Mendez, L. H. Philipson and R. F. Ismagilov, *Proc. Natl. Acad. Sci. U. S. A.*, 2008, **105**, 16843–16848.
36 Y. Liu and R. F. Ismagilov, *Langmuir*, 2009, **25**, 2854–2859.
37 D. E. Cohen, T. Schneider, M. Wang and D. T. Chiu, *Anal. Chem.*, 2010, **82**, 5707–5717.
38 S.-Y. Jung, S. T. Retterer and C. P. Collier, *Lab Chip*, 2010, **10**, 2688–2694.
39 Y. Liu, S.-Y. Jung and C. P. Collier, *Anal. Chem.*, 2009, **81**, 4922–4928.
40 M. He, C. Sun and D. T. Chiu, *Anal. Chem.*, 2004, **76**, 1222–1227.
41 At longer times (up to 3 s), the formation of Ag granules could be seen in the droplet due to photoreduction from the tungsten lamp on the microscope, similar to that reported by ref. 6.
42 G. J. Janz, G. R. Lakshminarayanan, M. P. Klotzkin and G. E. Mayer, *J. Phys. Chem.*, 1966, **70**, 536–539.
43 The diffusion coefficient for the 50 nm diameter beads was calculated using the Einstein–Stokes equation: $D = kBT/6\pi\eta r$, $T = 298$ K, $\eta = 10^{-3}$ Pa s.
44 R. Sjöback, J. Nygren and M. Kubista, *Spectrochim. Acta, Part A*, 1995, **51**, L7–L21.
45 The monoanion has a quantum yield of 0.37. Upon excitation, the neutral and cationic species are converted to the monoanion with quantum yields of 0.30 and 0.18. From ref. 44.
46 F. Courtois, L. F. Olguin, G. Whyte, A. B. Theberge, W. T. S. Huck, F. Hollfelder and C. Abell, *Anal. Chem.*, 2009, **81**, 3008–3016.

